



Article

Humidity Sensitivity Behavior of $\text{CH}_3\text{NH}_3\text{PbI}_3$ Perovskite

Xuefeng Zhao , Yuting Sun, Shuyu Liu, Gaifang Chen, Pengfei Chen, Jinsong Wang, Wenjun Cao and Chunchang Wang *

Laboratory of Dielectric Functional Materials, School of Materials Science & Engineering, Anhui University, Hefei 230601, China; b51814003@stu.ahu.edu.cn (X.Z.); b51814004@stu.ahu.edu.cn (Y.S.); b51814001@stu.ahu.edu.cn (S.L.); b19201039@stu.ahu.edu.cn (G.C.); b19201035@stu.ahu.edu.cn (P.C.); b20301123@stu.ahu.edu.cn (J.W.); b20201064@stu.ahu.edu.cn (W.C.)

* Correspondence: ccwang@ahu.edu.cn

Abstract: The $\text{CH}_3\text{NH}_3\text{PbI}_3$ (MAPbI_3) powders were ground by PbI_2 and $\text{CH}_3\text{NH}_3\text{I}$ prepared by ice bath method. The humidity sensitive properties of an impedance-type sensor based on MAPbI_3 materials were systematically studied. Our results indicate that the MAPbI_3 -based sensor has superior sensing behaviors, including high sensitivity of 5808, low hysteresis, approximately 6.76%, as well as good stability. Water-molecule-induced enhancement of the conductive carrier concentration was argued to be responsible for the excellent humidity sensitive properties. Interestingly, the humidity properties can be affected by red light sources. The photogenerated carriers broke the original balance and decreased the impedance of the sensor. This work promotes the development of perovskite materials in the field of humidity sensing.

Keywords: humidity sensing; impedance-type sensors; organometallic halide perovskite



Citation: Zhao, X.; Sun, Y.; Liu, S.; Chen, G.; Chen, P.; Wang, J.; Cao, W.; Wang, C. Humidity Sensitivity Behavior of $\text{CH}_3\text{NH}_3\text{PbI}_3$ Perovskite. *Nanomaterials* **2022**, *12*, 523. <https://doi.org/10.3390/nano12030523>

Academic Editor: Sergey Ya. Istomin

Received: 14 December 2021

Accepted: 31 January 2022

Published: 2 February 2022

Publisher's Note: MDPI stays neutral with regard to jurisdictional claims in published maps and institutional affiliations.



Copyright: © 2022 by the authors. Licensee MDPI, Basel, Switzerland. This article is an open access article distributed under the terms and conditions of the Creative Commons Attribution (CC BY) license (<https://creativecommons.org/licenses/by/4.0/>).

1. Introduction

Perovskites with the formula of AMX_3 (where A stands for an organic group or inorganic cation with twelve neighboring, X is a halide anion, and M is a metal cation) have been evidenced to be exciting solar absorber materials [1]. Besides the light harvesting performance, these compounds have recently demonstrated several intriguing properties, such as high dielectric constant [2], ferroelectricity [3], photorestriction [4], resistive switching [5], and optical cooling [6]. However, the AMX_3 perovskites suffer from the major obstacle of chemical and structural instability because they are sensitive to environmental factors. Previous work indicated that the perovskite lattice can interact with the polar water molecules due to the formation of strong hydrogen bonds between water molecules and the halide lattice [7]. This characteristic makes the properties of AMX_3 heavily dependent on the environment moisture. For example, Alberto García-Fernández et al. [8] investigated the electric properties of $\text{CH}_3\text{NH}_3\text{PbI}_3$ (MAPbI_3) in wet and dry environments. The results showed that both capacitance and conductivity in wet condition were several orders of magnitude larger than those in dry condition. This humidity sensitive feature gives the materials tremendous promise as probes for sensing of humidity. Truly, outstanding humidity performances of large sensitivity, remarkable fast response/recovery time, small hysteresis loop, and good linearity were reported in humidity sensors based on Cs_2PdBr_6 [9], $\text{CH}_3\text{NH}_3\text{PbI}_{3-x}\text{Cl}_x$ [10,11], $\text{Cs}_2\text{BiAgBr}_6$ [12], and CsPbBr_3 [7].

MAPbI_3 , being an important member of the AMX_3 family, has properties that strongly depend on environment humidity [8], indicating that it can be used as a humidity sensing material. Although humidity detection by MAPbI_3 was attempted by Ilin and co-authors [13], details about its humidity performances have not been studied. Additionally, because of the low-cost solution-based method and cheaper CH_3NH_2 , perovskite MAPbI_3 is less expensive than most humidity sensing materials such as CsPbBr_3 [14], Cs_2PdBr_6 [9], and $\text{Cs}_2\text{BiAgBr}_6$ [12]. Moreover, it was proved that illumination could lead to a giant dielectric

constant of lead halide perovskite [2]. Hence, we herein present a systematical investigation on the humidity performances of an impedance-type humidity sensor based on MAPbI₃.

In this work, MAPbI₃ was fabricated by grinding CH₃NH₃I made from an ice bath with PbI₂. The humidity sensing performance of the humidity sensor based on perovskite MAPbI₃ were tested at room temperature in the range of 11–94% relative humidity. Our results show that the MAPbI₃-based humidity sensor exhibits high humidity sensitivity performance. The possible mechanism of the humidity sensitivity and photoinduced changes were also discussed.

2. Materials and Methods

2.1. Powder Preparation

Methylamine iodide (MAI) was synthesized from 24 mL methylamine (MA) solution and 10 mL hydroiodic acid (HI) solution [15]. MA solution and HI solution were firstly mixed in a smaller beaker that was placed in a larger beaker at 0 °C. The mixed solution was continuously stirred in an ice bath for 120 min until evenly mixed to form a slightly yellowish solution. Then, the resulting mixture was evaporated in a vacuum oven at 90 °C for 7 h until a white precipitate was obtained. After naturally cooling down to room temperature, the obtained precipitate was washed 3 to 4 times with ether in a centrifuge. Eventually, the precipitate was dried at 60 °C for 24 h to obtain white crystalline powder MAI.

Preparation of lead methyl iodide triiodide (MAPbI₃). An equal molar amount of MAI powder and PbI₂ powder were ground in an agate mortar for 20 min until a visually black powder was obtained.

2.2. Characterization of Materials

The crystalline phase composition and structure of all powders were examined by X-ray diffraction (XRD, Rigaku Smartlab Beijing Co. Beijing, China) using Cu K α radiation. The morphology of MAPbI₃ powders was analyzed by scanning electron microscope (SEM, Model S 4800, Hitachi Co, Tokyo, Japan). The possible ferroelectricity of MAPbI₃ was investigated by measuring polarization-electric field (*P-E*) hysteresis loop using a TF analyzer (MultiFerroicII, Radiant technologies Inc, Albuquerque, New Mexico). In doing so, Au top electrodes were sputtered onto the surface of MAPbI₃ film to form a sandwich structure of Au/MAPbI₃/Au. The ultraviolet photoelectron spectroscopy (UPS) measurement was carried out using He-I radiation (21.2 eV) in vacuum (10⁻⁸ mbar) to measure the highest filled energy level of valence band (VBM) of MAPbI₃ film. The sample was biased at -10 V for measurement in the secondary electron cut off region.

2.3. Humidity Sensor Fabrication and Performances Measurements

The MAPbI₃-based humidity sensor was fabricated by aerosol deposition method on Al₂O₃ substrate covered with Au interdigitated electrodes. Figure 1 presents the photo images of the Al₂O₃ substrate and fabricated sensor. The sensor fabrication processes are as follows: firstly, a little amount of MAPbI₃ powder was mixed with anhydrous ethanol, and ultrasound for 15 min to form a homogeneous paste. Then, the paste was uniformly sprayed onto a Al₂O₃ substrate using a 0.2 mm caliber spray pen (Sao Tome V130). Two copper wires were fixed on the electrodes with silver glue. Finally, the sensor was dried at 100 °C for 10 min and naturally cooled down to indoor temperature. The whole process of sample preparation was shown in Figure 2.

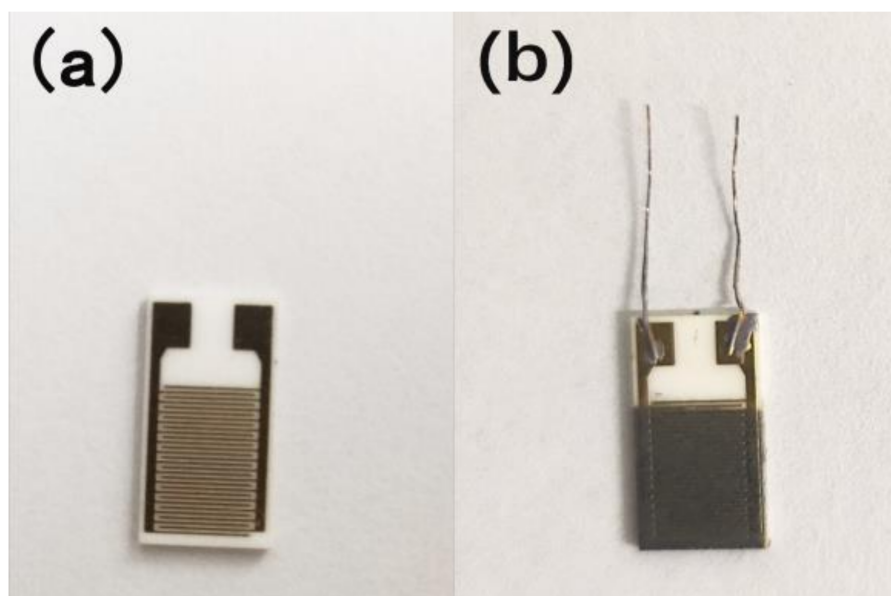


Figure 1. (a) Photo images of the Al_2O_3 substrate with Au interdigitated electrodes; and (b) the MAPbI_3 -based humidity sensor.

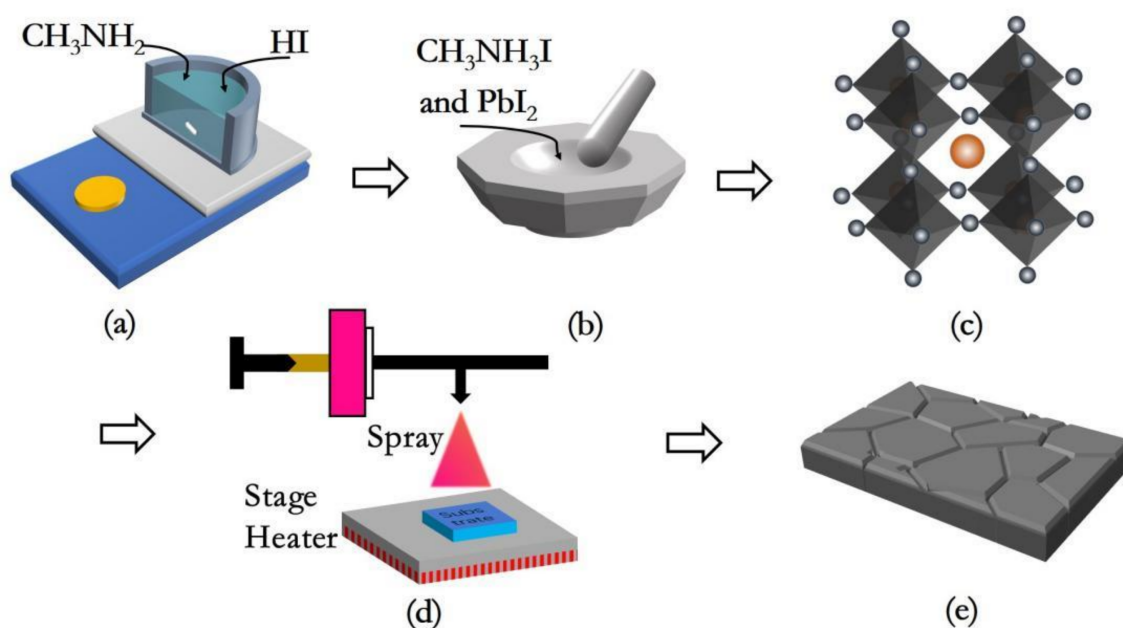


Figure 2. (a) Ice bath method; (b) grinding; (c) the structure of MAPbI_3 powder; (d) aerosol deposition method; and (e) the polycrystalline layer structure of MAPbI_3 thin film.

The different relative humidity (RH) environments were obtained by saturated salt solutions of LiCl , MgCl_2 , $\text{Mg}(\text{NO}_3)_2$, NaCl , KCl , and KNO_3 in closed containers. The environments above these solutions can provide RH levels of 11, 33, 54, 75, 85, and 94%, respectively. The impedance of the sensor was measured by an impedance analyzer (Hioki 3532-50 LCR). The experimental setup was illustrated in Figure 3. The influence of illumination on the MAPbI_3 -based sensor was reflected by impedance variation with and without light provided by 10 small red LED lights.

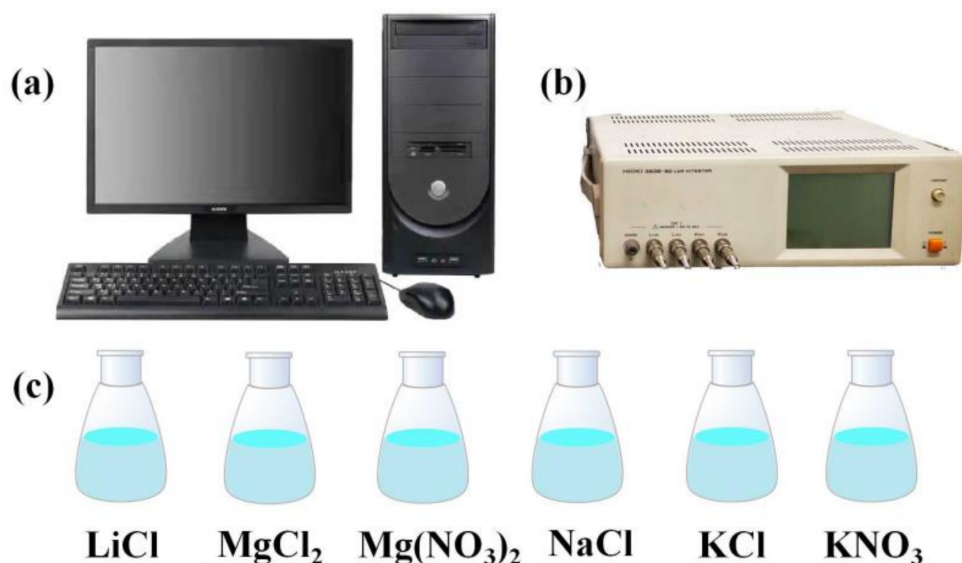


Figure 3. Schematic of the humidity sensing experimental setup: (a) PC; (b) Hioki 3532-50 LCR; and (c) different humidity environments.

3. Results

3.1. Structure and Morphology Characterizations

The XRD pattern of the MAPbI₃ powder was shown in the Figure 4a. The peaks at 14.1°, 28.4°, 31.7°, 40.5°, and 43.0° are assigned to (110), (220), (310), (224) and (314) planes, respectively. These peaks agree perfectly with MAPbI₃ perovskite tetragonal structure (The COD ID of MAPbI₃ is 2107954) [16]. The average grain size of the MAPbI₃ powder was clarified to be ~1.39 μm from the SEM image shown in the inset of Figure 4a. Figure 4b shows the *P-E* loops of the MAPbI₃ measured at room temperature with a frequency of 10 Hz under various voltages of 15, 30, and 45 V. The thickness of the film is 450 nm. The ellipse-shaped *P-E* loops indicate that the MAPbI₃ exhibits no ferroelectric behavior macroscopically at room temperature. This result is consistent with that reported in Refs. [3,17].

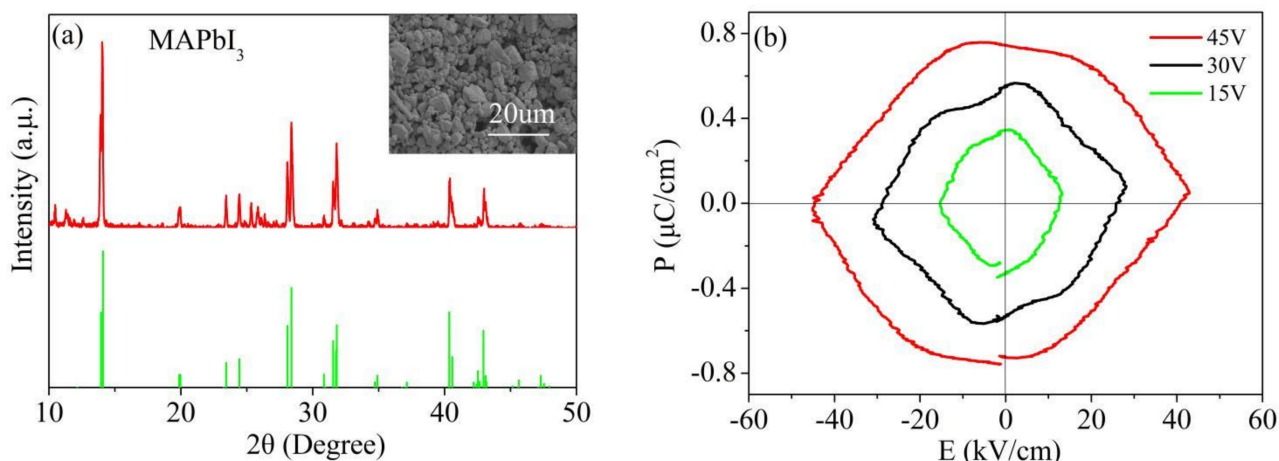


Figure 4. (a) XRD pattern and SEM image of MAPbI₃ powder; and (b) *P-E* loops of MAPbI₃ film measured at the frequency of 10 Hz under the voltage of 15, 30, and 45 V.

3.2. Humidity Sensitive Properties

The humidity sensitive performance of the MAPbI₃-based resistive sensor was studied by testing the impedance upon exposing the sensor to various RH levels with the a duration time of 5 min in each level. Figure 5a presents the impedance as a function of RH level of the MAPbI₃-based sensor at different frequencies. The impedance decreases with increasing measurement frequency. The curve measured with 100 Hz shows the largest impedance variation. Hence, 100 Hz is chosen as the optimum measuring frequency and will be used in the following part.

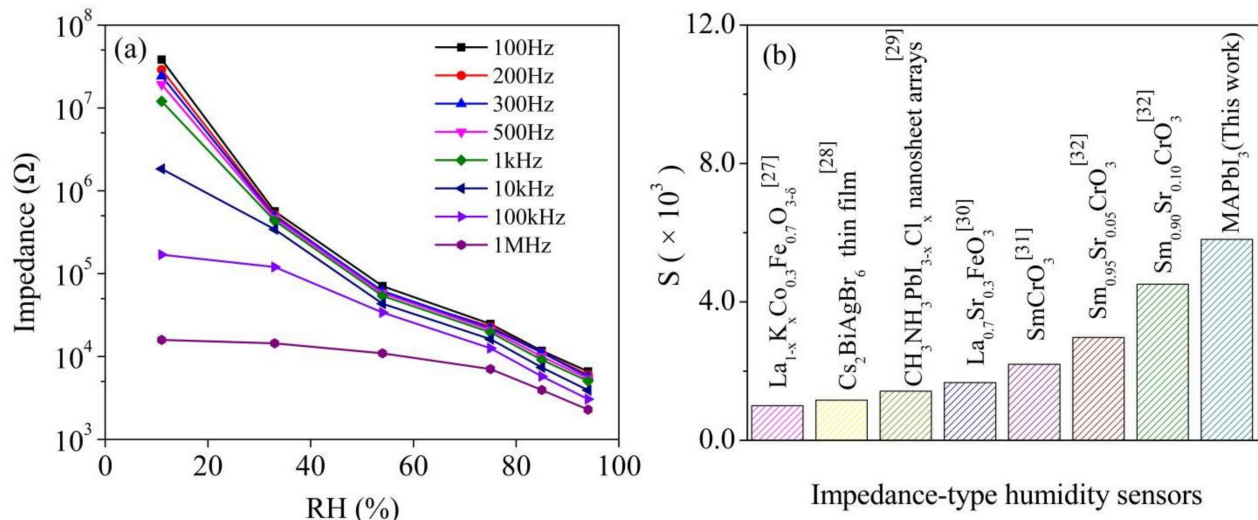


Figure 5. (a) The impedance as a function of RH level of the MAPbI₃-based sensor at different frequencies; (b) the contrast between the MAPbI₃-based sensor and other impedance-type humidity sensors in published literature.

Based on the data in Figure 5a, the humidity sensitive response (S) of the sensor can be calculated according to the relation [18,19]:

$$S = Z_d / Z_h \quad (1)$$

where Z_d and Z_h are the impedance values measured at 11%RH and at a specific RH level, respectively. The MAPbI₃-based sensor showed a superior sensitivity of $S = 5808$. Figure 5b displays a contrast of sensitive response between the MAPbI₃-based sensor and other impedance-type sensors reported in the literature [12,20–24]. The comparison highlights that the MAPbI₃ shows the largest sensitivity.

For the purpose of fully characterizing the performance of the MAPbI₃-based sensor, the hysteresis and recovery/response curves of the MAPbI₃-based sensor were tested at 100 Hz. The results were given in Figure 6a,b, respectively. The hysteresis curve was acquired by switching the sensor between the containers with the different RH levels of 11, 33, 54, 75, 85 and 94% in turn, and then shifting back. After an exposure duration of 5 min in each of the RH levels, the impedance was recorded under the optimum frequency of 100 Hz. Based on the measured impedance values, the humidity hysteresis values can be reckoned by the following formula [25]:

$$\left[\frac{\log(Z_{ads}) - \log(Z_{des})}{\log(Z_{ads})} \right] \times 100\% \quad (2)$$

where Z_{des} and Z_{ads} represent the impedance value of the desorption and the adsorption processes, respectively. A hysteresis value of 6.76% is obtained at 11%RH for the MAPbI₃-based sensor. The physical adsorption, which is toilless to be desorbed in MAPbI₃ material,

is much larger than the chemical adsorption that can be weakly influenced by environment humidity at low humidity level, which results in good hysteresis behavior of the sensor at low RH levels. Studies have shown that there is a steep increase in the water uptake in the RH level beyond 80%RH [26]. Therefore, the sensor still exhibits notable hysteresis under high humidity levels because the physical adsorption is greatly increased. Figure 6b displays the response and recovery time for the MAPbI₃-based sensor recorded between 11% and 94%RH. The result shows that the response and recovery times are 31 s and 148 s, respectively. Response/recovery time under other relative humidity levels are listed in Table 1.

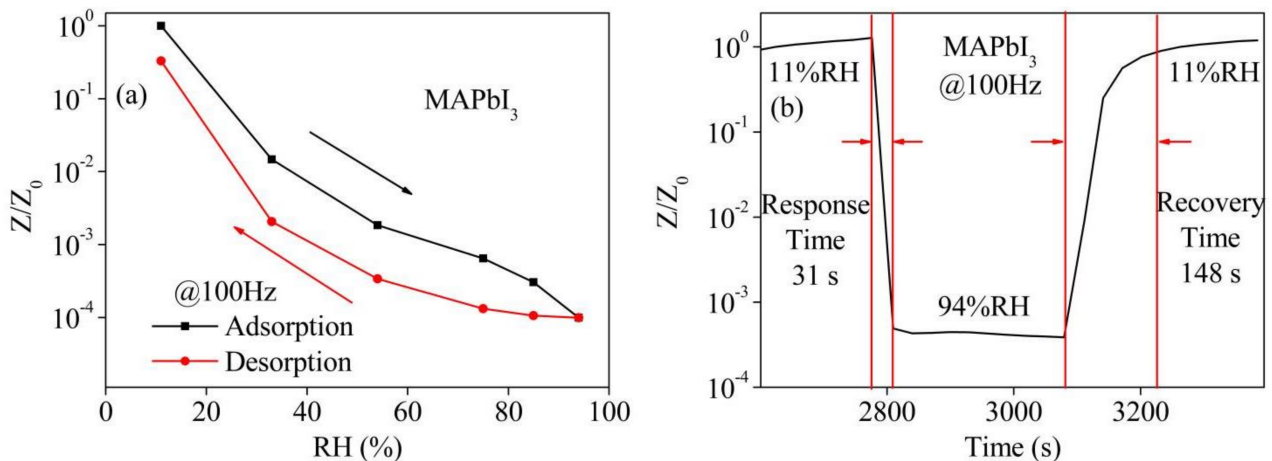


Figure 6. (a) Hysteresis behavior and (b) recovery/response time of the MAPbI₃-based sensor (Z/Z_0 is the normalized impedance to the initial impedance Z_0).

Table 1. Hysteresis and response/recovery time under different RH levels of the MAPbI₃-based sensor.

	Hysteresis	Response Time (s)	Recovery Time (s)
MAPbI ₃ -based sensor		64 (11%→33%)	90 (33%→11%)
		56 (11%→54%)	89 (54%→11%)
	Max = 18.61% (75%RH)	77 (11%→75%)	131 (75%→11%)
	Min = 6.76% (11%RH)	56 (11%→85%)	134 (85%→11%)
		31 (11%→94%)	148 (94%→11%)

The repeatability of the sensor was measured by switching the sensor between 11 and 94%RH levels for 5 cycles. The stability test was conducted over a period of 135 days. The results of repeatability and stability were shown in Figure 7a,b, respectively. After 5 cycles, the impedance under 11%RH remains 88.13% of the initial value, while under 94%RH, the impedance hardly changes. This result indicates that the sensor shows satisfactory repeatability. The impedance curves shown in Figure 7b remain almost constant, revealing that the sensor exhibits good long-term stability.

3.3. Influence of Light on the Humidity Sensing Properties

Previous work has indicated that red light affects the electric properties of MAPbI₃ [26]. To investigate the influence of illumination on the humidity sensing properties of the MAPbI₃-based sensor, 10 red LED lights were used as light source. The humidity sensor was placed in the environments of 11%, 54%, and 94%RH successively, and the impedance values were recorded during the three stages of darkness–lightness–darkness with the duration time of 300 s in each stage. The results were plotted in Figure 8. It is clearly shown that under a low humidity level of 11%RH, the impedance can be notably reduced by the light because the photogenerated carrier breaks the original carrier balance and increases the electron concentration, leading to the enhancement of electron conductivity. In the medium and high humidity levels, a similar situation of illumination-induced impedance

decrease to that of the low humidity level was observed when the lights were on. However, this impedance variation becomes much weaker than that in 11%RH. However, in the later stage of lighting, the electron concentration decreases due to electron–hole combination, so the impedance increases again. After the light source was switched off, considering that the non-equilibrium carriers does not disappear immediately, the impedance value increases at low and medium humidity levels due to the electron–hole interaction. However, impedance remarkably decreases at high humidity level, probably because the interaction between the light source and the continuous layer of water that forms on the surface of the sample.

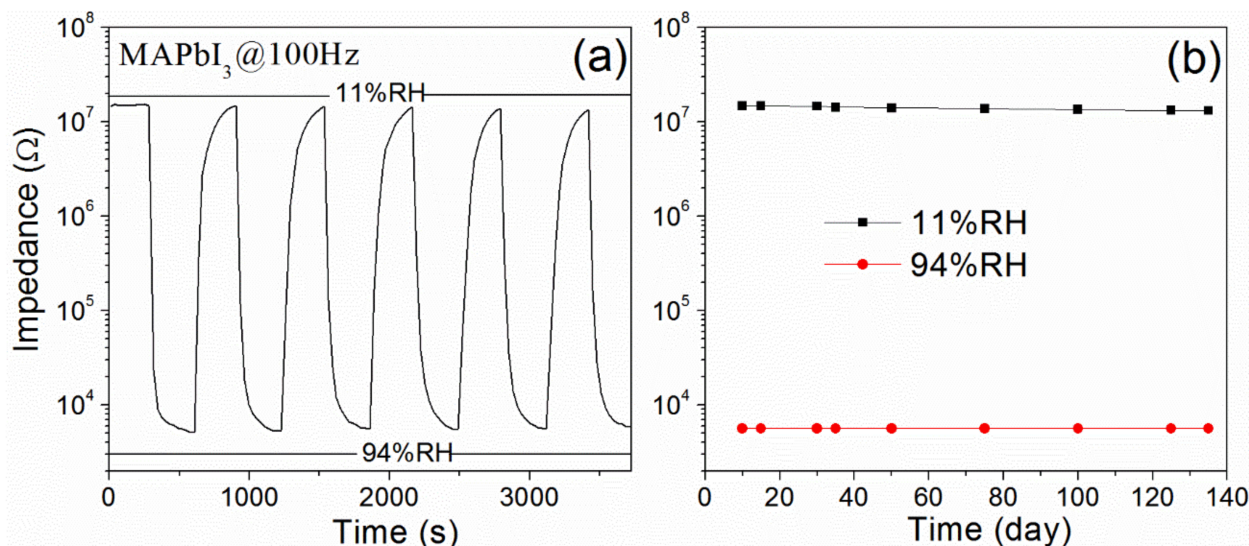


Figure 7. Repeatability (a) and long-term stability (b) of the MAPbI₃-based sensor.

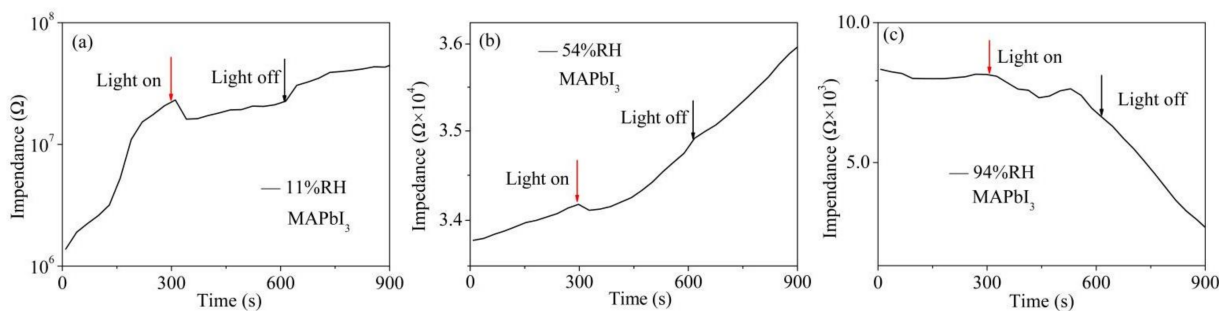


Figure 8. Illumination-induced impedance variations of the MAPbI₃-based sensor in the environment of (a) 11%, (b) 54%, and (c) 94%RH.

4. Discussion

To investigate the sensing mechanism, complex impedance diagrams of MAPbI₃-based sensor were measured with different RH levels. Figure 9 displays the complex impedance plots (Nyquist plots) obtained in different RH environments. At the low RH levels of 11 and 33%, the Nyquist plots are arc-like curves with large radius. The large radius indicates the high resistance at low humidity levels. The arc shrinks with the increasing of RH from 33% to 54%. A whole semicircle followed by a liner line in the low-frequency range is visible within the measuring frequency range when the RH beyond 75%RH. Further increasing the RH level, the semicircle becomes smaller, but the linear line becomes longer. This phenomenon indicates that both the resistance and reactance underwent a large decrease as the RH increases.

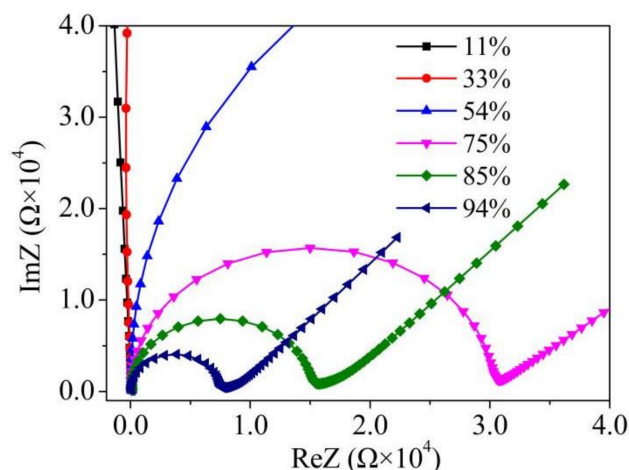


Figure 9. Complex impedance diagrams of the MAPbI₃-based sensor with different RH levels.

Previous work has manifested that the absorbed water molecules can deform the crystal lattice. As the content of water molecules increases to one molecule in one unit cell, this deformation becomes prominent, but the crystal structure is still not broken down [11]. This implies that perovskite materials have good capability accommodating water molecules. Figure 10a presents the UPS spectrum of the material, where the VBM is 1.35 eV below E_f , and its secondary electron truncation is located at 19.5 eV. In addition to the band gap value calculated from the absorption spectrum, the band structure is acquired and depicted in Figure 10b (the E_g of MAPbI₃ is 1.55 eV), where a standard n type feature could be concluded. With more water molecules absorbed by the structure, more electrons would be injected. This would lift the E_f of the material and enhance the conductivity of the material [11]. However, perovskite MAPbI₃ would form the hydrate-CH₃NH₃PbI₃·H₂O under high humidity [27]. It is clearly shown in Figure 5a that the impedance of MAPbI₃-based sensor decreases rapidly at low and moderate humidity levels, while the impedance value decreases slowly at high humidity level. Besides, the color of MAPbI₃-based sensor changes from black to yellow and then back to black when the sensor was successively exposed to 11, 94%RH and then back to 11%RH for 5 min at each RH level, which indicates the degradation is reversible. Therefore, under high humidity, most of the water molecules entering the crystal lattice were used to form hydrate, which leads to slow increase of electrons in the conduction band and slow increase of electrical conductivity. Moreover, due to the limitation of perovskite crystal structure, the hydrate formed is limited, so the electrical conductivity of this material increases slowly.

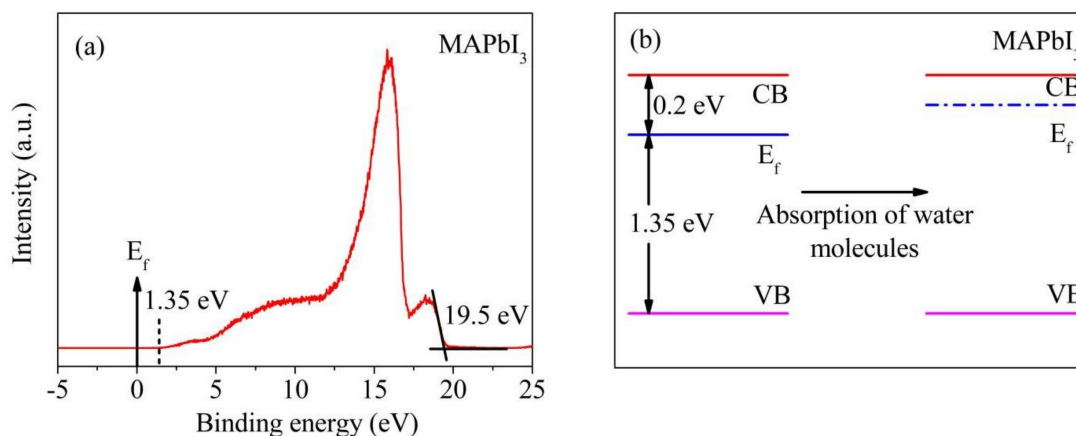


Figure 10. (a) The direct UPS spectrum of the as-grown bare MAPbI₃; and (b) the energy level diagrams of as-grown MAPbI₃ in the cases before and after absorbing water molecules.

5. Conclusions

In this work, we present investigation on the humidity properties on the MAPbI₃-based sensor. The results show that the sensor exhibits high sensitivity, superior to that of many perovskite materials. The humidity performances were argued to be caused by the fact that water molecules entered the perovskite lattice, serving as a strong *n*-type dopant that greatly enhances the concentration of conductive electrons. Our results emphasize that the MAPbI₃ perovskite has a great promise as humidity sensing material and could have widespread applications in humidity sensor.

Author Contributions: Conceptualization, X.Z. and Y.S.; methodology, S.L.; software, P.C.; validation, X.Z., Y.S. and S.L.; formal analysis, G.C.; investigation, X.Z.; resources, J.W.; data curation, X.Z.; writing—original draft preparation, X.Z.; writing—review and editing, C.W.; visualization, W.C.; supervision, C.W.; project administration, X.Z.; funding acquisition, C.W. All authors have read and agreed to the published version of the manuscript.

Funding: This research was funded by National Natural Science Foundation of China, grant number 51872001 and 12174001.

Institutional Review Board Statement: Not applicable.

Informed Consent Statement: Not applicable.

Data Availability Statement: The data is available on reasonable request from the corresponding author.

Conflicts of Interest: The authors declare no conflict of interest.

References

1. Ni, Z.Y.; Bao, C.X.; Liu, Y.; Jiang, Q.; Wu, W.Q.; Chen, S.S.; Dai, X.Z.; Chen, B.; Hartweg, B.; Yu, Z.S.; et al. Resolving spatial and energetic distributions of trap states in metal halide perovskite solar cells. *Science* **2020**, *367*, 1352–1358. [[CrossRef](#)] [[PubMed](#)]
2. Juarez-Perez, E.J.; Sanchez, R.S.; Badia, L.; Garcia-Belmonte, G.; Kang, Y.S.; Mora-Sero, I.; Bisquert, J. Photoinduced giant dielectric constant in lead halide perovskite solar cells. *J. Phys. Chem. Lett.* **2014**, *5*, 2390–2394. [[CrossRef](#)] [[PubMed](#)]
3. Fan, Z.; Xiao, J.X.; Sun, K.; Chen, L.; Hu, Y.T.; Quyan, J.Y.; Ong, K.P.; Zeng, K.Y.; Wang, J. Ferroelectricity of CH₃NH₃PbI₃ perovskite. *J. Phys. Chem. Lett.* **2015**, *6*, 1155–1161. [[CrossRef](#)] [[PubMed](#)]
4. Zhou, Y.; You, L.; Wang, S.W.; Ku, Z.L.; Fan, H.J.; Schmidt, D.; Rusydi, A.; Chang, L.; Wang, L.; Ren, P.; et al. Giant photostriction in organic-inorganic lead halide perovskites. *Nat. Commun.* **2016**, *7*, 11193. [[CrossRef](#)] [[PubMed](#)]
5. Zhang, X.H.; Zhao, X.N.; Shan, X.Y.; Tian, Q.L.; Wang, Z.Q.; Lin, Y.; Xu, H.Y.; Liu, Y.C. Humidity effect on resistive switching characteristics of the CH₃NH₃PbI₃ memristor. *ACS Appl. Mater. Inter.* **2021**, *13*, 28555–28563. [[CrossRef](#)] [[PubMed](#)]
6. Ha, S.T.; Shen, C.; Zhang, J.; Xiong, Q.H. Laser cooling of organic-inorganic lead halide perovskites. *Nat. Photonics* **2016**, *10*, 115–121. [[CrossRef](#)]
7. Cho, M.Y.; Kim, S.; Kim, I.S.; Kim, E.S.; Wang, Z.J.; Kim, N.Y.; Kim, S.W.; Oh, J.M. Perovskite-induced ultrasensitive and highly stable humidity sensor systems prepared by aerosol deposition at room temperature. *Adv. Funct. Mater.* **2019**, *30*, 1907449. [[CrossRef](#)]
8. García-Fernández, A.; Moradi, Z.; Bermúdez-García, J.M.; Sánchez-Andújar, M.; Gimeno, V.A.; Castro-García, S.; Señaris-Rodríguez, M.A.; Mas-Marzá, E.; Garcia-Belmonte, G.; Fabregat-Santiago, F. Effect of environmental humidity on the electrical properties of lead halide perovskites. *J. Phys. Chem. C* **2018**, *123*, 2011–2018. [[CrossRef](#)]
9. Ye, W.; Cao, Q.; Cheng, X.F.; Yu, C.; He, J.H.; Lu, J.M. Lead-free Cs₂PdBr₆ perovskite-based humidity sensor for artificial fruit waxing detection. *J. Mater. Chem. A* **2020**, *8*, 17675–17682. [[CrossRef](#)]
10. Hu, L.; Shao, G.; Jiang, T.; Li, D.B.; Lv, X.L.; Wang, H.Y.; Liu, X.S.; Song, H.S.; Tang, J.; Liu, H. Investigation of the interaction between perovskite films with moisture via in situ electrical resistance measurement. *ACS Appl. Mater. Inter.* **2015**, *7*, 25113–25120. [[CrossRef](#)]
11. Ren, K.K.; Huang, L.; Yue, S.Z.; Lu, S.D.; Liu, K.; Azam, M.; Wang, Z.J.; Wei, Z.M.; Qu, S.C.; Wang, Z.G. Turning a disadvantage into an advantage: Synthesizing high-quality organometallic halide perovskite nanosheet arrays for humidity sensors. *J. Mater. Chem. C* **2017**, *5*, 2504–2508. [[CrossRef](#)]
12. Weng, Z.H.; Qin, J.J.; Umar, A.A.; Wang, J.; Zhang, X.; Wang, H.L.; Cui, X.L.; Li, X.G.; Zheng, L.R.; Zhan, Y.Q. Lead-free Cs₂BiAgBr₆ double perovskite-based humidity sensor with superfast recovery time. *Adv. Funct. Mater.* **2019**, *29*, 1902234. [[CrossRef](#)]
13. Ilin, A.S.; Forsh, P.A.; Martyshov, M.N.; Kazanskii, A.G.; Forsh, E.A.; Kashkarov, P.K. Humidity sensing properties of organometallic perovskite CH₃NH₃PbI₃. *Chemistryselect* **2020**, *5*, 6705–6708. [[CrossRef](#)]

14. Wu, Z.L.; Yang, J.; Sun, X.; Wu, Y.J.; Wang, L.; Meng, G.; Kuang, D.L.; Guo, X.Z.; Qu, W.J.; Du, B.S.; et al. An excellent impedance-type humidity sensor based on halide perovskite CsPbBr₃ nanoparticles for human respiration monitoring. *Sens. Actuators B Chem.* **2021**, *337*, 129772. [[CrossRef](#)]
15. Jassim, S.M.; Bakr, N.A.; Mustafa, F.L. Synthesis and characterization of MAPbI₃ thin film and its application in C-Si/perovskite tandem solar cell. *J. Mater. Sci. Mater. Electron.* **2020**, *31*, 16199–16207, Correction in **2020**, *31*, 16208. [[CrossRef](#)]
16. Yang, J.L.; Yu, Y.; Zeng, L.Y.; Li, Y.T.; Pang, Y.Q.; Huang, F.Q.; Lin, B.L. Effects of aromatic ammoniums on methyl ammonium lead iodide hybrid perovskite materials. *J. Nanomater.* **2017**, 1640965. [[CrossRef](#)]
17. Li, W.W.; Zeng, J.G.; Zheng, L.Y.; Zeng, H.R.; Li, C.B.; Kassiba, A.; Park, C.; Li, G.R. Apparent ferroelectric-like and dielectric properties of CH₃NH₃PbI₃ synthesized in ambient air. *Ferroelectrics* **2019**, *553*, 95–102. [[CrossRef](#)]
18. Patil, D.; Seo, Y.K.; Hwang, Y.K.; Chang, J.S.; Patil, P. Humidity sensitive poly (2,5-dimethoxyaniline)/WO₃ composites. *Sens. Actuators B Chem.* **2008**, *132*, 116–124. [[CrossRef](#)]
19. Suri, K.; Annapoorni, S.; Sarkar, A.K.; Tandon, R.P. Gas and humidity sensors based on iron oxide-polypyrrole nanocomposites. *Sens. Actuators B Chem.* **2002**, *81*, 277–282. [[CrossRef](#)]
20. Wang, Z.Y.; Shi, L.Y.; Wu, F.Q.; Yuan, S.; Zhao, Y.; Zhang, M.H. Structure and humidity sensing properties of La_{1-x}K_xCo_{0.3}Fe_{0.7}O_{3-δ} perovskite. *Sens. Actuators B Chem.* **2011**, *158*, 89–96. [[CrossRef](#)]
21. Yao, P.J.; Wang, J.; Ji, M. Study on dielectric and humidity sensing properties of La_{1-x}Sr_xFeO₃ materials. *Ferroelectrics* **2010**, *402*, 79–88. [[CrossRef](#)]
22. Rao, M.C.; Srikumar, T.; Satish, D.V.; Krishna, J.S.R.; Rao, C.S.; Rao, C.R. Effect of zinc stannate nanofiller on PVA-CH₃COONa polymer electrolyte for humidity sensor application. *AIP Conf. Proc.* **2018**, *1992*, 040022.
23. Farahani, H.; Wagiran, R.; Urban, G.A. Investigation of room temperature protonic conduction of perovskite humidity sensors. *IEEE Sens. J.* **2020**, *21*, 9657–9666. [[CrossRef](#)]
24. Sundaram, R.; Raj, E.S.; Nagaraja, K.S. Microwave assisted synthesis, characterization and humidity dependent electrical conductivity studies of perovskite oxides, Sm_{1-x}Sr_xCrO₃ (0 ≤ x ≤ 0.1). *Sens. Actuators B Chem.* **2004**, *99*, 350–354. [[CrossRef](#)]
25. Lin, W.D.; Liao, C.T.; Chang, T.C.; Chen, S.H.; Wu, R.J. Humidity sensing properties of novel graphene/TiO₂ composites by sol-gel process. *Sens. Actuators B Chem.* **2015**, *209*, 555–561. [[CrossRef](#)]
26. Haque, M.A.; Syed, A.; Akhtar, F.H.; Shevate, R.; Singh, S.; Peinemann, K.V.; Baran, D.; Wu, T. Giant humidity effect on hybrid halide perovskite microstripes: Reversibility and sensing mechanism. *ACS Appl. Mater. Inter.* **2019**, *11*, 29821–29829. [[CrossRef](#)]
27. Prochowicz, D.; Franckevičius, M.; Cieślak, A.M.; Zakeeruddin, S.M.; Grätzel, M.; Lewiński, J. Mechano-synthesis of the hybrid perovskite CH₃NH₃PbI₃: Characterization and the corresponding solar cell efficiency. *J. Mater. Chem. A* **2015**, *3*, 20772–20777. [[CrossRef](#)]